Fizika Nizkikh Temperatur, 2000, v. 26, Nos. 9/10, p. 992–1000

Reactions of laser-ablated aluminum atoms with nitrogen during condensation at 10 K. Infrared spectra and density functional calculations for Al_xN_y molecular species

Lester Andrews, Mingfei Zhou*, George V. Chertihin, William D. Bare

Chemistry Department, P. O. Box 400319, University of Virginia, Charlottesville, VA 22904-4319, USA
E-mail: lsa@virginia.edu

Yacine Hannachi

Laboratoire de Physico-Chimie Moleculaire (CNRS UMR 3805), Universite Bordeaux I, 351, Cours de la Liberation, F-33405 Talence, Cedex France

Received February 11, 2000

Laser-ablated aluminum atoms react with dinitrogen on condensation at 10 K to form N_3 radical and the subject molecules, which are identified by nitrogen isotopic substitution, further reactions on annealing, and comparison with isotopic frequencies computed by density functional theory. The major AlN_3 product is identified from three fundamentals and a statistically mixed nitrogen isotopic octet pattern. The aluminum rich Al_2N and Al_3N species are major products on annealing to allow diffusion and further reaction of trapped species. This work provides the first experimental evidence for molecular Al_xN_y species that may be involved in ceramic film growth.

PACS: 81.15.Fg, 82.30.Cf

Introduction

Aluminum nitride is an important semiconductor and ceramic material [1], which has led to numerous investigations of the solid material [2] and its formation by chemical vapor deposition (CVD) from reactions of aluminum alkyls [3,4]. The only molecular aluminum nitride investigated, AlN, has been observed by emission [5] and investigated by post-Hartree Fock ab initio calculations [6,7]. In order to prepare Al_xN_y species of relevance to the CVD process, laser-ablated Al atoms have been reacted with ammonia [8]. Such compounds have been modeled by electronic structure calculations [9].

A recent investigation of laser-ablated Ga atoms reacting with nitrogen revealed a series of Ga_xN_y species that increase stepwise on annealing to allow diffusion and reaction to form Ga_3N and GaN_3 in a manner that might approximate gallium nitride film growth [10]. The stability of similar Al_3N and AlN_3 molecules has been verified by recent electronic structure calculations [11]. However, investigations of the B/N_2 reaction revealed NBNN as the most abundant product [12,13]. Here follows a combined matrix infrared spectroscopic and density functional theoretical study of novel Al_xN_y molecular species.

Experimental and computational methods

The technique for laser ablation and infrared matrix investigation has been described previously [12,14,15]. The aluminum target (Aesar, 99.998%) was mounted on a rotating rod. The 1064 nm Nd : YAG laser beam (Spectra Physics, DCR-11) was focused on the metal target. Laser energies ranging from 20–60 mJ/pulse were used in the experiments. Ablated aluminum atoms were codepo-

*Permanent address: Laser Chemistry Institute, Fudan University, Shanghai, P. R. China

sited with pure nitrogen onto a 10 K CsI window at a rate of 2–4 mmol/h for 30 min to 2 h. Nitrogen (Matheson) and isotopic $^{15}N_2$ (Isotec), $^{14}N_2 + {}^{15}N_2$, and $^{14}N_2 + {}^{14}N^{15}N + {}^{15}N_2$ (Isotec) mixtures were employed. Infrared spectra were recorded with 0.5 cm^{-1} resolution and 0.1 cm^{-1} accuracy on a Nicolet 750 instrument. Matrix samples were annealed to different temperatures, and selected samples were subjected to broadband photolysis by a medium pressure mercury arc lamp (Philips, 175W) with globe removed (240–580 nm).

Density functional theory (DFT) calculations were done for potential product molecules expected here using the Gaussian 94 program [16]. Most calculations employed the hybrid B3LYP functional but comparisons were done with the BP86 functional as well [17,18]. The 6-311+G* basis set was used for both Al and N atoms [19], and the cc-pVDZ set was employed in several computations [20]. Geometries were fully optimized and frequencies were calculated from analytic second derivatives.

Results

Infrared spectra and density functional calculations of aluminum-nitrogen reaction products will be presented in turn.

Infrared spectra. Matrix isolation infrared experiments were done on a 10 K salt window with laser-ablated aluminum and pure nitrogen. Representative infrared spectra are illustrated in Figs. 1, 2 and 3 for Al in pure nitrogen for three regions, and the product absorptions are listed in Table 1.

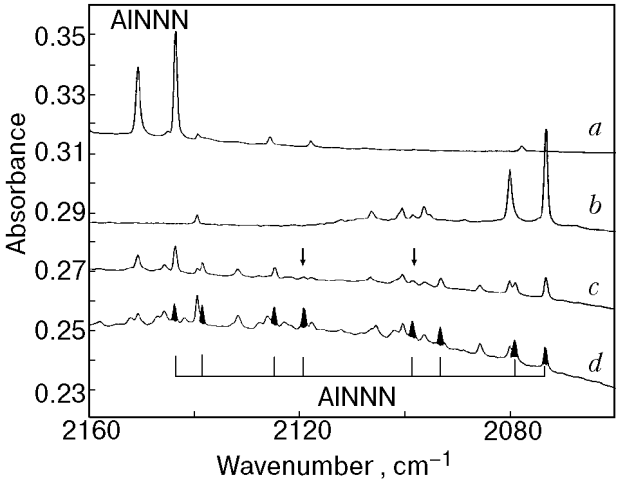

Fig. 1. Infrared spectra in the 2160–2060 cm^{-1} region for pure nitrogen isotopic samples codeposited with laser-ablated Al atoms after annealing to 25 K. (a) $^{14}N_2$, (b) $^{15}N_2$, (c) 50% $^{14}N_2$ + + 50% $^{15}N_2$, and (d) 25% $^{14}N_2$ + 50% $^{14}N^{15}N$ + 25% $^{15}N_2$ (major site octet indicated).

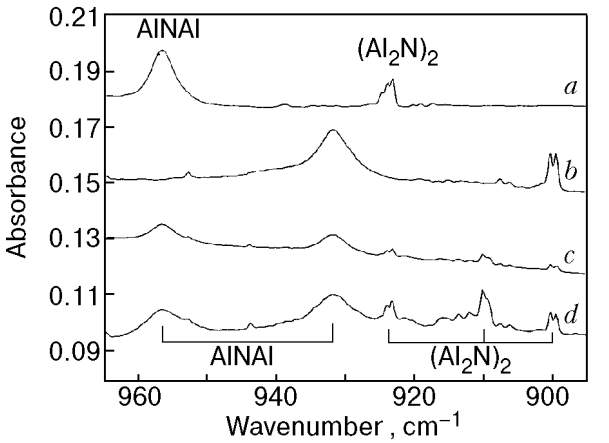

Fig. 2. Infrared spectra in the 965–895 cm^{-1} region for same pure nitrogen isotopic samples as in Fig. 1.

The strong N_3 radical [12,21] absorption at 1657.7 cm^{-1} (not shown) is 13 times stronger than the N_3^- band at 2003.3 cm^{-1}. As a measure of limited oxide contamination, the NO band at 1874.7 cm^{-1} is very weak (absorbance $A = 0.001$, not shown) and trace Al_2O is detected at 988.7 cm^{-1} ($A = 0.005$) [22]. The major aluminum product absorbs at 2150.9/2144.0 cm^{-1}, 1391.9/1386.0 cm^{-1}, and 509.7 cm^{-1} (not shown) with $A = 0.036$, 0.006, and 0.004, respectively. Another product has bands at 1501.6 and 956.7 cm^{-1}, another at 777.9/770.3 cm^{-1}, and different products absorb at 656.9 and 650.7 cm^{-1}. Finally, an experiment with the lowest laser energy used here markedly reduced the 956.7 and 779.9/770.3 cm^{-1} bands relative to other products.

Similar experiments were done with $^{15}N_2$, and the shifted bands are reported in Table 1. Analogous investigations with $^{14}N_2 + {}^{15}N_2$ and $^{14}N_2 + {}^{14}N^{15}N + {}^{15}N_2$ mixed isotopic samples gave impor-

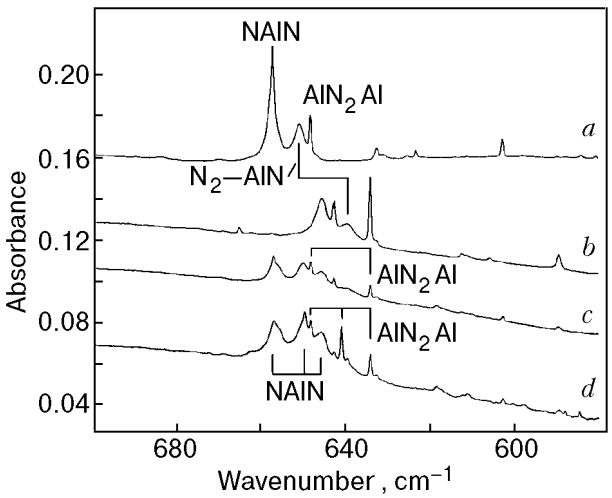

Fig. 3. Infrared spectra in the 700–580 cm^{-1} region for same pure nitrogen isotopic samples as in Fig. 1.

Table 1

Infrared absorptions (cm^{-1}) for laser-ablated Al atom reactions with pure N_2 during condensation at 10 K

$^{14}N_2$	$^{15}N_2$	$^{14}N_2 + {}^{14}N^{15}N + {}^{15}N_2$	$^{14}N_2/{}^{15}N_2$	Identification
2327.6	2250.3	2327.6, 2289.6, 2250.3	1.03435	N_2
2178.4	2106.5		1.03413	$(N_2–AlNNN)$
2172.3	2100.6		1.03413	$(N_2–AlNNN)$
2167.9	2096.4	weak intermediate bands	1.03411	$(N_2–AlNNN)$
2150.9	2080.1		1.03404	AlNNN site
2144.0	2073.2	2144.0, 2138.7, 2125.1, 2119.4, 2098.8, 2093.4, 2079.5, 2073.4	1.03415	AlNNN
2077.8	2009.6		1.03394	$X–N_3^-$
2003.3	1837.5	2003.2, 1992.7, 1981.7, 1959.4, 1948.7, 1937.4	1.03396	N_3^-
1874.7	1841.8		1.01786	NO
1657.7	1603.5	1657.7, 1649.3, 1640.0, 1621.5, 1613.0, 1603.5	1.03380	N_3
1501.6	1474.9	1501.6, 1474.9	1.01810	AlNAl
1391.9	1345.4		1.03456	AlNNN site
1386.0	1340.2	weak intermediate bands	1.03417	AlNNN
1132.8	1106.0		1.02423	Al_xN_y
1126.8	1100.4		1.02399	Al_xN_y
1061.9	1040.7		1.02037	Al_xN_y
1054.3	1033.4		1.02022	Al_xN_y
956.7	931.7	956.7, 931.7	1.02683	AlNAl
923.2	899.4	923.2, 909.2, 899.4	1.02646	$(Al_2N)_2$
777.9	758.6	777.9, 758.6	1.02544	Al_3N
770.3	751.2	770.3, 751.2	1.02540	Al_3N
680.0	664.9	680.0, 773.0, 664.9	1.02271	$Al_xN_y–(N_2)_x$
656.9	645.4	656.9, 649.5, 645.4	1.01782	NAlN
650.7	636.5	650.7, 636.5	1.02231	$N_2–AlN$
648.2	634.0	648.2, 640.8, 634.0	1.02240	Al_2N_2
632.7	612.3	632.7, 618.2, 612.3	1.03332	Al_xN_y
623.6	605.8	624, 610, 606	1.02872	Al_xN_y
602.6	589.4	602.6, 589.4	1.02240	Al_xN_y
509.7	501.5		1.01635	AlNNN
486.7	472.5	486.7, 472.5	1.03005	Al_xN_y

tant diagnostic multiplets. Isotopic spectra are compared in Figs. 1–3 and the multiplet absorptions are listed in Table 1.

Calculations. Langhoff et al. have performed CASSCF and MRCI calculations on the $^3\Pi$ ground state of AlN and found 744 cm^{-1} and 1.816 Å, and 746 cm^{-1} and 1.813 Å harmonic frequency and bond length, respectively [7]. Our B3LYP/6-311+G* calculation gave 730 cm^{-1} and 1.805 Å for the AlN ground state, which are in very good agreement and

Table 2

Calculated (B3LYP/6-311+G*) geometry, frequencies (cm^{-1}) and intensities (km/mol) for the AlN, Al_2N, Al_3N, NAlN, NAlNN, AlNNN, and Al_2N_2 molecules

Molecule	Geometry	Frequencies (Intensities)
AlN ($^3\Pi$)	Al–N: 1.805 Å	730.1 (12) 713.9 (12)[a]
Al_2N ($^2\Sigma_u^+$)	Al–N: 1.731 Å Linear	131.8 (35), 524.9 (0), 1051.4 (97) 128.3 (33), 524.9 (0), 1023.3 (92)[a]
Al_2N ($^2\Sigma_u^+$)	Al–N: 1.748 Å Linear	77.7 (2×15), 509.2 (0), 1004.3 (72)[b] 75.6, 509.2, 977.4[a,b]
Al_2N^- ($^1\Sigma_g^+$)	Al–N: 1.746 Å Linear	119.0 (2×2), 518.7 (0), 1129.8 (685) 115.8 (1×2), 518.7 (0), 1099.5 (643)[a]
Al_3N ($^1A_1$) C_{2v}	Al_1N: 1.8495 Å $Al_{2,3}N$: 1.850 Å $\angle Al_2–N–Al_3$: 120.1°	153.8 (3), 154.3 (3), 217.0 (0), 427.5 (0), 751.5 (328), 751.9 (329) 153.2 (3), 153.8 (3), 210.8 (0), 427.5 (0), 732.4 (312), 732.8 (314)[a]
Al_3N ($^1A_1'$)D_{3h}	Al–N: 1.863 Å	141.1 (3×2), 200.6 (0.1), 414.3 (0), 731.9 (309×2)[c]
NAlN ($^4\Pi_u$)	Al–N: 1.804 Å Linear	122.2 (43), 146.2 (86), 643.2 (0), 725.7 (582) 120.2 (41), 143.8 (83), 621.5 (0), 713.8 (563)[a]
NAlNN ($^1A'$)	N–Al: 1.746 Å Al–N: 2.021 Å N–N: 1.106 Å N–Al–N: 87.1° Al–N–N: 177.7°	89.8 (47), 230.6 (4), 259.0 (17), 326.4 (12), 840.1 (21), 229.6 (381)
AlNNN ($^1\Sigma^+$)	Al–N: 1.826 Å N–N: 1.206 Å N–N: 1.138 Å	94.4 (2), 497.4 (167), 625.4 (17), 626.4 (18), 1466.0 (320), 2271.2 (1018), 91.6 (2), 490.8 (162), 604.2 (16), 605.2 (17), 1416.9 (301), 2194.4 (950)[a]
N_3^- ($^1\Sigma_g^+$)	1.1832 Å	628.2 (7×2), 1351.8 (0), 2078.5 (1241)
AlN_2Al ($^3\Sigma_g^-$)	Al–N: 1.860 Å N–N: 1.204 Å	82.2 (2), 257.7 (0), 369.2 (0), 634.3 (579), 1739.4 (0)
AlN_2Al ($^3\Sigma_g^-$)	Al–N: 1.888 Å N–N: 1.204 Å	78.4 (1×2), 224.9 (0×2), 355.9 (0), 612.0 (509), 1757.1 (0)[b] 76.7 [π_u], 217.5 [π_g], 355.9 [π_g], 598.5 [σ_u], 1697.8 [σ_g][a,b]
$(AlN)_2$ (^1A_g)	Al–N: 2.041 Å N–N: 1.267 Å	160.4 (0.2), 195.3 (21), 337.0 (0), 554.2 (0), 571.5 (509), 1445.9 (0) 156.9 (0.2), 191.0 (20), 337.0 (0), 536.5 (0), 558.9 (487), 1396.8 (0)[a]
$(AlN)_2$ (^1A_g)	Al–N: 2.074 Å N–N: 1.263 Å	156 (0), 193 (18), 331 (0), 553 (0), 564 (463), 1453 (0)[b]

[a]Frequencies for ^{15}N substitution, [b]cc-pVDZ basis set, [c]BP86 functional; (2×2) is to denote doubly degenerate mode of intensity 2, etc.

serve to «calibrate» the calculations reported here. The B3LYP/cc-pVDZ calculation gave 717 cm^{-1} and 1.821 Å for AlN.

Three isomers were considered for Al_2N including a triangle, AlAlN, and AlNAl. The $^2\Sigma_u^+$ AlNAl species was the most stable (the C_{2v} form is 54.5 kcal/mol higher and the $C_{\infty v}$ structure 76.6 kcal/mol higher at the B3LYP/cc-pVDZ level). Table 2 shows that the cc-pVDZ set gave slightly longer (0.017 Å) bonds and a 47 cm^{-1} lower antisymmetric stretching frequency than the 6-311G* set for Al_2N. The Al_2N molecule has a high computed Al–N–Al frequency near that for Al–O–Al.

Following our work with boron where NBNN was the major product species [12,13], we calculated NAlNN, and found ($^1A'$) NAlNN to be

Table 3

Calculated (B3LYP/cc-pVDZ) relative energies (kcal/mol) geometries, frequencies (cm^{-1}), and intensities (km/mol) for Al_4N_2 molecules

Symmetry	Energy	Lengths, angles	Frequencies (Intensities)[a]
C_s	0.0	$Al_{1,2}$–N_1: 1.879 Å N_1–Al_3 : 1.810 Å Al_3–N_2 : 1.693 Å N_2–Al_4: 1.791 Å $Al_{1,2}$–N_1–Al_3 : 116.9° N–Al–N: 179.3° Al_3–N_2–Al_4: 164.3°	a': 245 (17), 355 (2), 532 (116), 814 (127), 1153 (504) a'': 723 (334) 239, 353, 528, 794, 1126[b] 704[b]
C_{2v} , $^1A_1$	28.5	Al_1–N_1: 2.065 Å Al_3–N_2 : 1.846 Å N_1–N_2 : 1.439 Å N_1–Al_1–N_2 : 40.8° N_1–N_2–Al_3 : 165.6° Al_1–N_1N_2–Al_2: 125.1°	a_1: 311 (41), 387 (3), 1067 (8) a_2: 212 (0), b_1: 506 (267) 308, 386, 1033[b] 200, 495, 205, 648[b]
$D_{\infty h}$, $^1\Sigma_g^+$	39.1	Al_1–Al_2 : 2.554 Å Al_1–N_1 : 1.690 Å N_1–Al_3 : 1.810 Å	σ_g : 545 (0), 1154 (0) σ_u : 499 (126), 1132 (803) 544, 1126, 499, 1103[b]
C_s , $^3A'$	44.7	$Al_{1,2}$–N_1: 1.887 Å N_1–Al_3 : 1.794 Å Al_3–N_2 : 1.700 Å N_2–Al_4 : 1.787 Å Al_2–N_1–Al_3 : 136.2° Al_1–N_1–Al_3 : 135.6° Al_3–N_2–Al_4 : 144.1°	a': 223 (30), 372 (45), 543 (45) 595 (17), 230 (883), 1086 (220) a'': 243 (38) 186, 222, 369, 531, 580, 860, 1061, 238[b]
D_2 , $^3B_2$	78.6	Al–N: 1.925 Å N–N: 1.369 Å Al_1–NN–Al_3 : 69.7°	a_1 : 338 (0), 962 (0) b_1 : 217 (0), 493 (10) b_2 : 217 (17), 525 (59) b_3 : 287 (239), 603 (222) 338, 930, 211, 482[b] 210, 514, 286, 588[b]

[a] All real frequencies; only those above 200 cm^{-1} listed; [b] $^{15}N^{15}N$ substituted frequencies.

73.0 kcal/mol *above* ($^1\Sigma^+$) AlNNN aluminum azide presumably owing to weaker Al–N bonds. Our results for AlNNN (Table 2) are in accord with recent MP2 calculations [11]. Similar B3LYP calculations were done with NBNN and BNNN for comparison, and the boron azide is 34.0 kcal/mol higher. The BNNN stretching frequencies are 2324 cm^{-1} (742 km/mol), 1519 (536) and 979 (128). Also following our observation of NBN [12], the aluminum analog was calculated to have a $^4\Pi_u$ ground state.

After finding Al_2N to be a stable radical, the saturated Al_3N molecule was computed to be very stable. The Al–N bond lengths and highest frequencies (B3LYP) suggest that the molecule is essentially trigonal planar, in agreement with higher level calculations [11].

Six structures of formula Al_4N_2 that might result from the dimerization of Al_2N radicals were calculated at the B3LYP/cc-pVDZ level and the results are summarized in Table 3. The two lowest energy structures are shown in Fig. 4. The global minimum has a plane of symmetry, and a strong infrared absorbing frequency calculated at 1153 cm^{-1}. The C_{2v} bridged structure is 28.5 kcal/mol higher and has lower frequencies. The linear species is 39.1 kcal/mol higher, but it has a strong fundamental calculated at 1132 cm^{-1}. The coplanar (C_{2v})

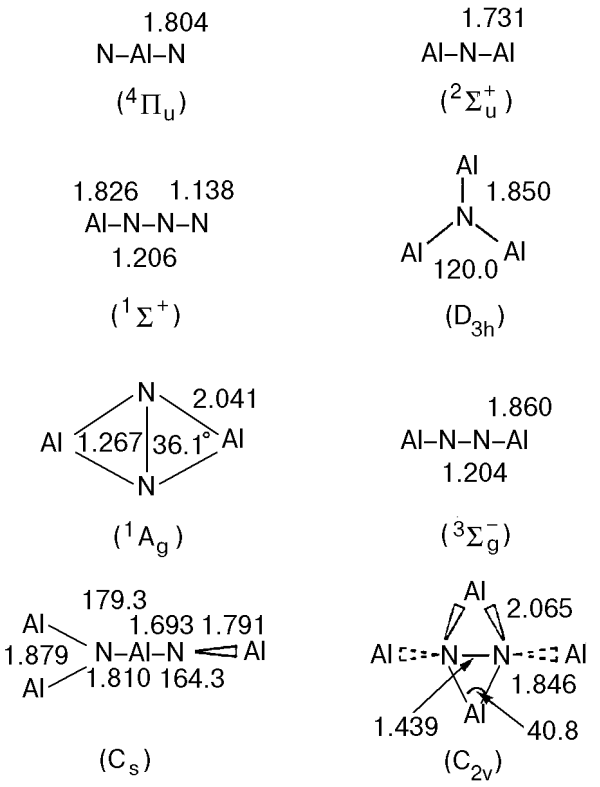

Fig. 4. Optimized geometries of Al_xN_y products computed by B3LYP/6-311+G*. Bond lengths in Å and angles in degrees. Al_4N_2 structures calculated with cc-pVDZ basis set.

version of the global minimum is 95.1 kcal/mol higher and is not listed.

Figure 4 illustrates the geometries of important Al_xN_y species.

Discussion

The new product absorptions will be identified from isotopic shifts, splitting patterns, and density functional isotopic frequency calculations.

AlN. The first product to be considered is AlN; the gas phase fundamental is 746.8 cm^{-1} and theoretical calculations sustain this assignment [5–7]. Although the 670–760 cm^{-1} region contains no significant absorption, a 650.7 cm^{-1} band grows slightly on annealing and almost disappears on photolysis. This band shows a 14/15 isotopic frequency ratio of 1.02231, which is just below the harmonic Al–N diatomic ratio of 1.02264. Furthermore, the 650.7 cm^{-1} band exhibits a doublet in mixed isotopic spectra providing evidence for a single N atom vibration. The gas phase-to-nitrogen-matrix shift is excessive for an isolated molecule so we believe a better assignment for the 650.7 cm^{-1} band is to a perturbed AlN molecule. We note that AlN is a $^3\Pi$ state and that both NAlNN and AlN_3 are singlet states. Although AlNNN (see below) increases on annealing, there is no evidence for the higher energy NAlNN isomer. Perhaps the perturbation is at the metal center, i.e. NN–AlN.

The AlN molecule is prepared here by direct reaction (1) between the atoms, which is

$$Al + N \rightarrow AlN \qquad (\Delta E = -60 \text{ kcal/mol}) \qquad (1)$$

calculated (B3LYP without ZPE) to be exothermic. The presence of N atoms in these experiments is confirmed by observation of the N_3 radical [12,21].

AlN_3. The major aluminum product in solid nitrogen absorbs at 2150.9/2144.0 cm^{-1}, 1391.9/1386.0 cm^{-1}, and 509.7 cm^{-1}. These bands increase 10% on 25 K annealing, almost disappear on 240–580 nm photolysis, reproduce in part on subsequent 30 K annealing, and increase more on 35 K annealing. The observed intensities are 0.0379/0.0074/0.0061 a.u. after 25 K annealing. The diagnostic mixed isotopic pattern for the strong higher frequency band is a sextet with $^{14}N_2 + {}^{15}N_2$ and an octet with $^{14}N_2 + {}^{14}N^{15}N + {}^{15}N_2$ (Fig. 1, arrows mark positions of Al-15-14-15 and Al-14-15-14 isotopic bands unique to the statistically mixed isotopic experiment). These sextet and octet patterns are much clearer for the GaNNN species where annealing increases one matrix site and removes the other [10]; nevertheless these multiplets identify the vibration of three inequivalent nitrogen atoms.

Since this band is in the azide stretching region, AlN_3 was investigated by DFT and found to be a stable $^1\Sigma^+$ molecule (Table 2). The three strong stretching fundamentals are calculated at 2271.2, 1466.0, and 497.4 cm^{-1} with 6/2/1 relative intensities. Scale factors of 0.947 and 0.949 are required to fit the upper two N–N stretching modes and 1.025 to fit the lower Al–N stretching mode. The same calculation predicted the strong N_3^- mode at 2078.5 cm^{-1}, which requires a 0.964 scale factor and is appropriate for the B3LYP functional [23]. The relative intensities are also modeled reasonably well by the B3LYP functional except the intensity of the weaker symmetric N–N–N stretching mode is overestimated relative to the stronger antisymmetric N–N–N stretching mode. The calculated and observed 14/15 isotopic ratios match and verify the normal mode assignments. Similar agreement between experiment and theory was found for GaN_3 [10]. The gas phase observation of CaN_3 and SrN_3, our matrix formation of the MN_3 (M = Al, Ga, In, Tl) molecules, and the synthesis of $Al(N_3)_3$ show that these azides are physically stable molecules [10,24,25].

Two mechanisms for the formation of AlN_3 come to mind, the reaction of Al with N_3 radical, and the

AlN reaction with N_2, the strongly exothermic (B3LYP) reactions (2a) and (2b):

$$Al + N_3 \rightarrow AlN_3 \quad (\Delta E = -94 \text{ kcal/mol}) , \quad (2a)$$

$$AlN + N_2 \rightarrow AlN_3 \quad (\Delta E = -49 \text{ kcal/mol}) . \quad (2b)$$

Mixed $^{14}N_2 + {}^{15}N_2$ isotopic spectra can in principle distinguish between these two reactions, but complications from two matrix site absorptions reduce the accuracy of band intensity measurements. However, for GaN_3, the mixed isotopic spectra were clearly resolved for the major site absorption, and it was suggested that about 80% of the GaN_3 product is formed from the N_3 radical reaction [10].

NAlN. The strong 656.9 cm^{-1} band also increased on annealing and decreased markedly on photolysis. This band showed a small $^{14}N_2/{}^{15}N_2$ ratio (1.01782) and an approximate 1:2:1 triplet pattern with $^{14}N_2 + {}^{14}N{}^{15}N + {}^{15}N_2$, which is characteristic of *two equivalent* N atoms (Fig. 3). In fact the 14/15 isotopic ratio for the harmonic antisymmetric vibration of a linear N–Al–N unit is 1.01673. Our B3LYP calculations find a stable linear NAlN molecule ($^4\Pi_u$ state) with σ_u frequency at 725.7 cm^{-1}, in very good agreement with the matrix observation. The slightly higher observed 14/15 ratio might suggest slight bending of the molecule in the matrix. The scale factor 0.905 required to fit the calculated and observed bands is lower than other comparisons reported here; this suggests that higher level calculations might provide a better description of the $^4\Pi_u$ state of NAlN.

The NAlN molecule is formed by the reaction of N with the metal center in AlN, reaction (3), which is exothermic. However, NAlN is higher energy than Al + N_2 by 120 kcal/mol

$$N + AlN \rightarrow NAlN \ (^4\Pi_u) \quad (\Delta E = -44 \text{ kcal/mol}) \quad (3)$$

(B3LYP), but NAlN clearly is kinetically stable. Even Al–N_2 is a van der Waals molecule (bound 4 kcal/mol as estimated by B3LYP).

The analogous NGaN molecule was observed at 586.4, 584.1 cm^{-1} (^{69}Ga, ^{71}Ga) where resolved isotopic splitting confirmed the vibration of a single gallium atom [10].

AlNAl. The 956.7 cm^{-1} band increases slightly on annealing but almost *doubles* on photolysis. The mixed isotopic spectra reveal a doublet absorption (Fig. 2) for the vibration of *a single* nitrogen atom and a large (1.02683) nitrogen 14/15 isotopic ratio. In fact the 14/15 isotopic ratio for the harmonic antisymmetric vibration of a linear Al–N–Al unit is 1.02750. Our B3LYP calculation finds the most stable Al_2N species to be linear AlNAl ($^2\Sigma_u^+$) with calculated σ_u mode at 1051.4 cm^{-1}, in very good agreement with the matrix spectrum. The scale factor 0.910 again suggests that higher level calculations might produce a better fit, and indeed the cc-pVDZ basis set (Table 2) produces a 1004.3 cm^{-1} σ_u frequency in better agreement with the observed value (0.953 scale factor). The 956.7 cm^{-1} band is assigned to AlNAl in solid nitrogen.

The sharp 1501.6 cm^{-1} band tracks with the 956.7 cm^{-1} band on annealing and photolysis, and it too shows the doublet mixed isotopic spectrum for the vibration of *a single* nitrogen atom. Its appearance in the NO region and 14/15 isotopic ratio invited consideration of such a species but AlNO and AlON absorb elsewhere [26]. The differences 1501.6 – 956.7 = 544.9 cm^{-1} and 1474.9 – – 931.7 = 543.2 cm^{-1} for the ^{15}N counterpart provide a mode that shows *very little* ^{15}N*-shift* and is near the 524.9 cm^{-1} calculated value for the σ_g mode of AlNAl. A slight amount of bending of the molecule would decrease the 14/15 ratio of the σ_u mode and increase the 14/15 ratio of the σ_g mode. Although the 1501.6 cm^{-1} band absorbance (0.008) is larger relative to the 956.7 cm^{-1} band (0.014) than normally found for a combination band and a fundamental, linear molecules often have relatively strong combination bands, and the 1501.6 cm^{-1} band is assigned to the $\sigma_u + \sigma_g$ combination band for AlNAl.

Similar experiments with laser-ablated Al atoms and 4% N_2 in argon reveal weak 981.3, 974.8 cm^{-1} bands with the same isotopic behavior that can be assigned to AlNAl in solid argon [27]. This suggests a matrix shift for the pure nitrogen environment, and the argon matrix bands clearly fit the DFT frequency calculations better.

The sequential reactions of Al atoms with AlN are exothermic, based on our B3LYP calculations:

$$AlN + Al \rightarrow AlNAl \quad (\Delta E = -114 \text{ kcal/mol}) , \quad (4)$$

$$AlNAl + Al \rightarrow Al_3N \quad (\Delta E = -86 \text{ kcal/mol}) . \quad (5)$$

Al_3N. Two sharp bands at 777.9, 770.3 cm^{-1} also increased slightly on annealing, but markedly on photolysis, more on subsequent annealing, and remained strong after 35 K annealing in contrast to AlNAl, which almost disappeared. Only the same pure isotopic bands were observed in mixed isotopic experiments so again *a single* nitrogen atom is involved. These bands exhibited virtually the same isotopic 14/15 ratio, 1.02542 ± 0.00002, which is

slightly smaller than the above 956.7/931.7 ratio for AlNAl. Hence, the 777.9, 770.3 cm^{-1} bands are also due to an antisymmetric Al–N–Al stretching mode, with a slightly smaller included angle, and the product may involve further Al reaction with AlNAl.

Our B3LYP and BP86 and recent higher level calculations [11] show that Al_3N is stable, and the strong e' mode predicted at 751.7 cm^{-1} with 14/15 ratio 1.02606 is extremely close to the observed value. The 777.9, 770.3 cm^{-1} bands are assigned to the e' mode of Al_3N split by interaction with the nitrogen matrix.

The major product in argon matrix experiments [27] at 773.1 cm^{-1} increases and remains on annealing to 40 K. The sharp doublet with mixed isotopic precursor and the 1.02547 isotopic frequency ratio show that this is the same Al_3N species observed in the nitrogen matrix. Finally, the observation of a single band for the e' mode of Al_3N in solid argon shows that the splitting in the nitrogen matrix is environmental and suggests that the split mode in the B3LYP calculation is due to symmetry breaking inherent in the calculation [28]. The D_{3h} symmetry of the molecule maintained with the pure density functional BP86 (Table 2) is also expected in the gas phase.

Al_3N. The anomalously low electron affinity recently measured for Al_3N is characteristic of a closed-shell molecule [29], which is calculated to be very stable [30]; these observations are in accord with the matrix infrared spectrum and behavior reported here for Al_3N.

Al_2N_2 . The most stable Al_2N_2 isomer is the ($^1A_1'$) rhombic ring [11], and this characteristic $(AlN)_2$ structure exhibits diatomic isotopic ratios. However, the linear AlNNAl molecule is only 1.8 kcal/mol higher at the B3LYP level with both basis sets, and the σ_u mode also exhibits the diatomic isotopic ratio. The sharp 648.2 cm^{-1} band meets these requirements: a 1.02240 isotopic ratio and a triplet with $^{14}N_2 + {}^{14}N^{15}N + {}^{15}N_2$ for *two equivalent* nitrogen atoms. The b_{1u} mode of the singlet rhombus is predicted at 571.5 cm^{-1} whereas the σ_u mode of triplet AlNNAl is 634.3 cm^{-1} (Table 2). Clearly, the latter fits the 648.2 cm^{-1} band more closely, and it is assigned accordingly.

Note, however, that a strong 648.2, 634.0 cm^{-1} doublet is observed with $^{14}N_2 + {}^{15}N_2$ indicating that *a single dinitrogen* molecule is reacting to form AlNNAl. Although Al–N_2 is only a van der Waals molecule, another Al atom will react to give the stable AlNNAl product,

$$Al + N_2 + Al \rightarrow AlNNAl \ (\Delta E = -42 \text{ kcal/mol}), \quad (6)$$

reaction (6), which is 42 kcal/mol exothermic.

$(Al_2N)_2$. Both nitrogen and argon matrix experiments [27] contain a weak band near 924 cm^{-1} that grows on annealing and remains at the end of annealing cycles. These bands form 1:2:1 triplets in *both* mixed isotopic experiments so *two equivalent* nitrogen atoms from *different* nitrogen molecules are required. The 14/15 ratios 1.0264 also denote an antisymmetric Al–N–Al vibration of a nearly linear Al–N–Al subunit. The annealing behavior suggests a high Al/N species. The 924 cm^{-1} band is tentatively assigned to an Al_2N dimer. Unfortunately, none of the Al_4N_2 calculations (Table 3) fit particularly well, but this is a difficult system to calculate.

Higher Al_xN_y absorptions. The nitrogen matrix experiments contain bands at 1132.8, 1126.8, 1061.9 and 1054.3 cm^{-1}, which increase on annealing and show 14/15 isotopic ratios near the diatomic AlN value. Unfortunately, no mixed isotopic data can be obtained from this congested spectral region. The 1132.8, 1126.8 cm^{-1} bands are destroyed by photolysis while the 1061.9, 1054.3 cm^{-1} bands increase and remain on final annealing. Clearly, these bands are due to higher Al_xN_y clusters. In this regard a linear AlNAlAlNAl chain has a very strong stretching mode predicted at 1132 cm^{-1}, which suggests that Al_xN_y chains absorb in this region.

Conclusions

Laser-ablated aluminum atoms react with dinitrogen on condensation at 10 K to form N_3 radical and the AlN_2 , Al_2N, Al_2N_2 , AlN_3 and Al_3N molecules, which are identified by nitrogen isotopic substitution, further reactions on annealing, and comparison with isotopic frequencies computed by density functional theory. The major AlN_3 product is identified from three fundamentals and a statistically mixed nitrogen isotopic octet pattern. The aluminum rich Al_2N and Al_3N species are major products on annealing to allow diffusion and further reaction of trapped species. This work provides the first experimental evidence for molecular Al_xN_y species that may be involved in ceramic film growth.

Acknowledgment

We gratefully acknowledge partial research support from the N.S.F., P.R.F. and C.N.R.S.

1. T. J. Morz, Jr., *Ceram. Bull.* **70**, 849 (1991).
2. See for example: K. Miwa and A. Fukumoto, *Phys. Rev.* **B48**, 789 (1993); E. Ruiz, S. Alvarez, and P. Alemarz, *Phys. Rev.* **B94**, 7115 (1994); A. K. Knudsen, *Bull. Am. Ceramic Soc.* **74**, 97 (1995); R. Y. Krupitskaya and G. W. Auner, *J. Appl. Phys.* **84**, 2861 (1998); G. T. Kiehne, G. K. L. Wong, and J. B. Ketterson, *J. Appl. Phys.* **84**, 5922 (1998).
3. *Chemistry of Aluminum, Gallium, Indium and Thallium*, A. J. Downs (ed.), Chapman and Hall, New York (1993).
4. A. Y. Timoshkin, H. F. Bettinger, and H. F. Schaefer, III, *J. Am. Chem. Soc.* **119**, 5668 (1997).
5. J. D. Simmons and J. K. McDonald, *J. Mol. Spectrosc.* **41**, 584 (1972).
6. M. Pelissier and J. P. Malrieu, *J. Mol. Spectrosc.* **77**, 322 (1979).
7. S. R. Langhoff, C. W. Bauschlicher, Jr., and L. G. M. Petterson, *J. Chem. Phys.* **89**, 7354 (1988).
8. D. V. Lanzisera and L. Andrews, *J. Phys. Chem.* **A101**, 5082 (1997).
9. R. D. Davy and K. L. Jaffrey, *J. Phys. Chem.* **98**, 8930 (1994).
10. M. F. Zhou and L. Andrews, *J. Phys. Chem.* **A104**, 1648 (2000).
11. B. H. Boo and Z. Liu, *J. Phys. Chem.* **A103**, 1250 (1999).
12. P. Hassanzadeh and L. Andrews, *J. Phys. Chem.* **96**, 9177 (1992).
13. L. Andrews, P. Hassanzadeh, T. R. Burkholder, and J. M. L. Martin, *J. Chem. Phys.* **98**, 922 (1993).
14. T. R. Burkholder and L. Andrews, *J. Chem. Phys.* **95**, 8697 (1991).
15. L. Andrews, T. R. Burkholder, and J. T. Yustein, *J. Phys. Chem.* **96**, 10182 (1992).
16. M. J. Frisch, G. W. Trucks, H. B. Schlegel, P. M. W. Gill, B. G. Johnson, M. A. Robb, J. R. Cheeseman, T. Keith, G. A. Petersson, J. A. Montgomery, K. Raghavachari, M. A. Al-Laham, V. G. Zakrzewski, J. V. Ortiz, J. B. Foresman, J. Cioslowski, B. B. Stefanov, A. Nanayakkara, M. Challacombe, C. Y. Peng, P. Y. Ayala, W. Chen, M. W. Wong, J. L. Andres, E. S. Replogle, R. Gomperts, R. L. Martin, D. J. Fox, J. S. Binkley, D. J. Defrees, J. Baker, J. P. Stewart, M. Head-Gordon, C. Gonzalez, and J. A. Pople, *Gaussian 94*, Revision B.1, Gaussian, Inc., Pittsburgh, PA (1995).
17. C. Lee, E. Yang, and R. G. Parr, *Phys. Rev.* **B37**, 785 (1988).
18. J. P. Perdew, *Phys. Rev.* **B33**, 8822 (1986); A. D. Becke, *J. Chem. Phys.* **98**, 5648 (1993).
19. A. D. Mclean and G. S. Chandler, *J. Chem. Phys.* **72**, 5639 (1980); R. Krishnan, J. S. Binkley, P. Seeger, and J. A. Pople, *J. Chem. Phys.* **72**, 650 (1980).
20. D. E. Woon and T. H. Dunning, Jr., *J. Chem. Phys.* **98**, 1358 (1993).
21. T. Tian, J. C. Facelli, and J. Michl, *J. Phys. Chem.* **95**, 8554 (1991).
22. S. M. Sonchik, L. Andrews, and K. D. Carlson, *J. Phys. Chem.* **87**, 2004 (1983) and references therein.
23. I. Bytheway and M. W. Wong, *Chem. Phys. Lett.* **282**, 219 (1998).
24. C. R. Brazier and P. F. Bernath, *J. Chem. Phys.* **88**, 2112 (1988).
25. C. J. Linnen, D. E. Macks, and R. D. Coombe, *J. Phys. Chem.* **B101**, 1602 (1997).
26. L. Andrews, M. F. Zhou, and W. D. Bare, *J. Phys. Chem.* **102**, 5019 (1998).
27. L. Andrews, M. F. Zhou, G. V. Chertihin, W. D. Bare, and Y. Hannachi, *J. Phys. Chem.* **A104**, 1656 (2000).
28. C. D. Sherill, M. S. Lee, and M. Head-Gordon, *Chem. Phys. Letts.* **302**, 425 (1999).
29. S. K. Nayak, B. K. Rao, P. Jena, X. Li, and L.-S. Wang, *Chem. Phys. Letts.* **301**, 379 (1999)
30. S. K. Nayak, S. N. Khanna, and P. Jena, *Phys. Rev.* **B57**, 3787 (1998).